

Band engineering of valleytronics WSe_2-MoS_2 heterostructures via stacking form, magnetic moment and thickness

Yanwei Wu(吴彦玮), Zongyuan Zhang(张宗源), Liang Ma(马亮), Tao Liu(刘涛) Ning Hao(郝宁), Wengang Lu(吕文刚), Mingsheng Long(龙明生) and Lei Shan(单磊)
Citation: Chin. Phys. B, 2023, 32 (**10**): 107506. DOI: 10.1088/1674-1056/acb761
Journal homepage: http://cpb.iphy.ac.cn; http://iopscience.iop.org/cpb

What follows is a list of articles you may be interested in

Prediction of a monolayer spin-spiral semiconductor: CoO with a honeycomb lattice

Jie Zhang(张杰), Shunuo Song(宋姝诺), Yan-Fang Zhang(张艳芳),Yu-Yang Zhang(张余洋), Sokrates T. Pantelides, and Shixuan Du(杜世萱)
Chin. Phys. B, 2023, 32 (**8**): 087508. DOI: 10.1088/1674-1056/acd923

Low-temperature ferromagnetism in tensile-strained $LaCoO_{2.5}$ thin film

Yang-Yang Fan(范洋洋), Jing Wang(王晶), Feng-Xia Hu(胡凤霞), Bao-He Li(李宝河), Ai-Cong Geng(耿爱丛), Zhuo Yin(殷卓), Cheng Zhang(张丞), Hou-Bo Zhou(周厚博), Meng-Qin Wang(王梦琴), Zi-Bing Yu(尉紫冰), and Bao-Gen Shen(沈保根)
Chin. Phys. B, 2023, 32 (**8**): 087504. DOI: 10.1088/1674-1056/acafdc

Doping-enhanced robustness of anomaly-related magnetoresistance in $WTe_{2\pm\alpha}$ flakes

Jianchao Meng(孟建超), Xinxiang Chen(陈鑫祥), Tingna Shao(邵婷娜), Mingrui Liu(刘明睿), Weimin Jiang(姜伟民), Zitao Zhang(张子涛), Changmin Xiong(熊昌民), Ruifen Dou(窦瑞芬), and Jiacai Nie(聂家财)
Chin. Phys. B, 2023, 32 (**4**): 047502. DOI: 10.1088/1674-1056/acb423

Enhanced and tunable Imbert-Fedorov shift based on epsilon-near-zero response of Weyl semimetal

Ji-Peng Wu(伍计鹏), Yuan-Jiang Xiang(项元江), and Xiao-Yu Dai(戴小玉)
Chin. Phys. B, 2023, 32 (**3**): 037503. DOI: 10.1088/1674-1056/ac7f92

Orbital torque of Cr-induced magnetization switching in perpendicularly magnetized Pt/Co/Pt/Cr heterostructures

Hongfei Xie(谢宏斐), Yuhan Chang(常宇晗), Xi Guo(郭玺), Jianrong Zhang(张健荣), Baoshan Cui(崔宝山), Yalu Zuo(左亚路), and Li Xi(席力)
Chin. Phys. B, 2023, 32 (**3**): 037502. DOI: 10.1088/1674-1056/aca6d7

SPECIAL TOPIC — Valleytronics

Band engineering of valleytronics WSe_2–MoS_2 heterostructures via stacking form, magnetic moment and thickness

Yanwei Wu(吴彦玮)[1,†], Zongyuan Zhang(张宗源)[1,‡], Liang Ma(马亮)[2], Tao Liu(刘涛)[1], Ning Hao(郝宁)[3], Wengang Lü(吕文刚)[4], Mingsheng Long(龙明生)[1], and Lei Shan(单磊)[1,§]

[1] *Information Materials and Intelligent Sensing Laboratory of Anhui Province, Key Laboratory of Structure and Functional Regulation of Hybrid Materials of Ministry of Education, Institutes of Physical Science and Information Technology, Anhui University, Hefei* 230601, *China*

[2] *State Key Laboratory of Metastable Materials Science & Technology and Key Laboratory for Microstructural Material Physics of Hebei Province, School of Science, Yanshan University, Qinhuangdao* 066004, *China*

[3] *Anhui Province Key Laboratory of Condensed Matter Physics at Extreme Conditions, High Magnetic Field Laboratory, Chinese Academy of Sciences, Hefei* 230031, *China*

[4] *Beijing National center for Condensed Matter Physics, Beijing Key Laboratory for Nanomaterials and Nanodevices, Institute of Physics, Chinese Academy of Sciences, Beijing* 100190, *China*

(Received 31 October 2022; revised manuscript received 20 January 2023; accepted manuscript online 31 January 2023)

Spin-valley polarization and bandgap regulation are critical in the developing of quantum devices. Here, by employing the density functional theory, we investigate the effects of stacking form, thickness and magnetic moment in the electronic structures of WSe_2–MoS_2 heterostructures. Calculations show that spin-valley polarization maintains in all situations. Increasing thickness of 2H-MoS_2 not only tunes the bandgap but also changes the degeneracy of the conduction band minimums (CBM) at K/K_1 points. Gradual increase of micro magnetic moment tunes the bandgap and raises the valence band maximums (VBM) at Γ point. In addition, the regulation of band gap by the thickness of 2H-MoS_2 and introduced magnetic moment depends on the stacking type. Results suggest that WSe_2–MoS_2 heterostructure supports an ideal platform for valleytronics applications. Our methods also give new ways of optical absorption regulation in spin-valley devices.

Keywords: valleytronics, thickness, stacking, magnetic moment

PACS: 21.60.Jz, 31.15.ej, 75.75.Lf, 71.20.–b **DOI:** 10.1088/1674-1056/acb761

1. Introduction

In the past years, two-dimensional (2D) materials have attracted many researchers' interest due to their particular magnetic,[1,2] electronic and optical properties.[3–7] For transition metal dichalcogenide (TMD) systems, when thinned down to monolayer, lots of new physical properties were discovered, such as the direct bandgap,[8,9] non-centrosymmetric crystal structure, and valley-contrasting optical selection rule.[10–13]

It is known that transition metal dichalcogenides (TMDs) with a honeycomb lattice such as MX_2 (M = Mo/W; X = S/Se) consist of hexagonal X–M–X covalently bonded quasi-2D structures. In monolayer situation, TMDs exhibit a direct bandgap which is in the visible frequency range. Owing to the inversion symmetry breaking and strong spin–orbit coupling, monolayer TMDs exhibit two inequivalent spin-valley polarized band edges at K and $-K$ points at the corners of the hexagonal Brillouin zone (BZ). As a new degree of freedom (DOF) beside spin and charge, circularly polarized light,[11–14] magnetic fields,[15,16] strain,[17] spin-polarized current[18] and magnetic proximity effect[19–21] can be used in valley regulation. Such attractive interaction between spin and valley pseudospin makes monolayer TMDs an ideal platform for spin manipulations, valley physics and valleytronics applications.

As a common method, the construction of heterostructures[22–24] is widely used in the tuning of band structure in 2D materials' applications. Former studies of vertical stacking van der Waals heterostructures have been successfully carried out. Applications and related theories have demonstrated the efficient interlayer electron transfer and tunable layer population of electrons and holes.[25–29] However, regulation of electronic structures of 2D materials is still critical and challenging. Many methods, such as dichalcogenides doped with magnetic transition metal atoms,[30–33] applying electric field,[34] adjusting temperature,[35] and strain regulation,[34,36,37] have been reported. In the method of temperature adjusting, the range of the bandgap tuning is very small ($\sim 10^{-1}$ meV/K). As for strain regulation, large shape variable is hard to achieve although the bandgap change is

†Corresponding author. E-mail: wywss433@126.com
‡Corresponding author. E-mail: zongyuanzhang@ahu.edu.cn
§Corresponding author. E-mail: lshan@ahu.edu.cn

© 2023 Chinese Physical Society and IOP Publishing Ltd

very considerable. Since spin–orbit coupling is not considered, methods such as applying external electron field and doping magnetic transition metal atom dichalcogenides[30–32] are independent of spin valley physics.

In this study, we have investigated the electronic structures of WSe_2–MoS_2 heterostructures in different stacking form and thickness. We combine the monolayer WSe_2 with monolayer (ML), bilayer (BL) and three layers (TL) 2H-MoS_2 in structure construction. In order to find the effect of the magnetic moment on band gap engineering, we have added a z-axis magnetic moment to different stacking WSe_2–MoS_2 heterobilayers. Results suggest that stacking form, thickness and magnetization are effective in the regulation of valleys' light absorption in WSe_2–MoS_2 heterostructures, providing new ideas of photoelectric applications in this valleytronics system. In addition, Ref. [38] has investigated the breaking of valley degeneracy in $MoSe_2$ monolayer by an out-plane magnetic field up to 6.7 T at 4.2 K, providing the feasibility of our ideas.

2. Methods

We perform all calculations by employing the Vienna *ab-initio* simulation package (VASP)[39–41] within the framework of the projector augmented wave (PAW) method. The generalized gradient approximation (GGA) parameters by Perdew–Burke–Ernzerhof (PBE)[42] are used as the exchange–correlations, van der Waals correction (DFT-D2) method[43] is accounted to describe the van der Waals interactions. To investigate the different stacking type, we adopt 2×2 unit cells for the structure construction. In geometry optimizing, we adopt 25 Å vacuums slabs for MX_2 (M = W/Mo, X = S/Se) monolayers while 20 Å vacuum slabs for WSe_2–MoS_2 heterobilayers. The cutoff energy of the plane-wave basis is set to 400 eV. A 10^{-5} eV electronic iteration convergence criterion with a 0.01 eV/Å force tolerance is set for all calculations for structure relaxing. For ML WSe_2–TL MoS_2 systems, we calculate these heterostructures by using real space projectors to reduce the computation. In addition, we use Gamma-centered 11×11×1 Monkhorst–Pack k-point sampling grid for geometry optimization and 13×13×1 for static self-consistency. Magnetic moment (0.03–0.15 μ_B) is added in z-direction to the supercell of all heterostructures. Spin–orbit coupling (SOC) is considered in all systems.

3. Results and discussion

3.1. Thickness and stacking forms of WSe_2–MoS_2 heterostructures

It is known that the monolayer MX_2 is in the form of X–M–X and consists a hexagonal of Mo/W layer sandwiched between two S/Se layers. The structure of 2H-MoS_2 is symmetrical in a hexagon, with two layers as a period, and forms a triangular prism coordination with Mo atom as the center (shown in Fig. 1(a)).

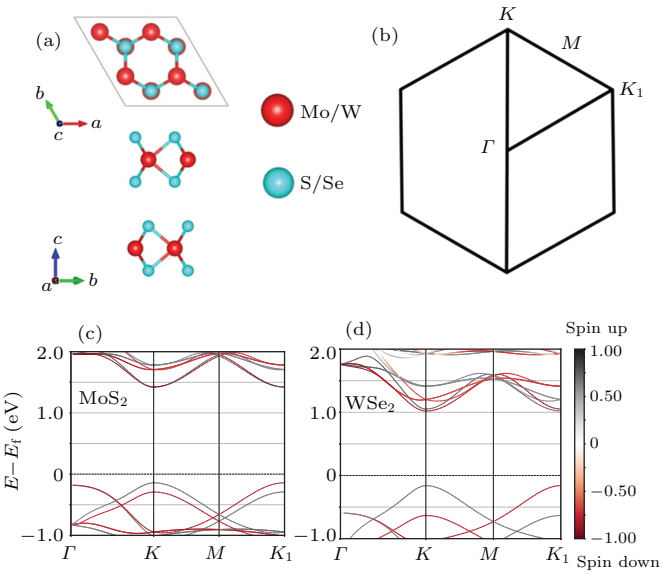


Fig. 1. (a) Top and side views of 2H-MX_2 (M = Mo/W, X = S/Se), (b) hexagonal Brillouin zone (BZ) and high symmetry points of 2D structure, (c) and (d) calculated band structures (with SOC) of monolayer MoS_2 and WSe_2.

We first consider the effect of different stacking on bandgap tuning of the heterostructures. As shown in Fig. 2, we have divided these heterostructures into six groups, which are called I, II, III, IV, V and VI. At the interface of all structures in the same group, WSe_2 and MoS_2 have the same stacked interlayer.

We have performed a calculation of the electronic structures for different stacked WSe_2-MoS_2 heterostructures to illustrate how the thickness affects the bandgap. Results are listed in Figs. 3, S1 and S2.

As shown in Figs. 3(a), S1 and S2, all stacking types have direct band gap and spin-valley polarization. In Fig. 3(b), the CBMs are mainly contributed by Mo in the MoS_2 layer(s), while the VBMs are mainly contributed by W of the WSe_2 monolayer. Due to the degenerated CBM, the valley index (K/K_1 point) is determined by the stacking direction of monolayer WSe_2, which is also indicated in Fig. S1 (types I, III and V have the same valley index, while types II, IV, VI possess the other consistent index). Raising thickness of 2H-MoS_2 increases both band gap and K/K_1 points' CBM degeneracy. To illustrate the results more precisely, we summarize the results in Table 1.

As shown in Table 1, our results suggest that the bandgaps of monolayer MoS_2 and WSe_2 agree well with previous studies.[34,44,45] Compared with MoS_2 and WSe_2 monolayers, the construction of WSe_2–MoS_2 heterobilayers reduces the bandgap with a maximum value of 1.308 eV. On this basis, the energy gap can be finely regulated by the layer thickness

and stacking mode of the heterojunction. Increasing the thickness of 2H-MoS_2 raises the bandgap in all stacking forms. Besides, the effect of band gap regulation also depends on the stacking type. Such tuning ranges suggest that the thickness of 2H-MoS_2 in the constructions of MoS_2–WSe_2 heterostructures has advantages in electronic devices (such as field effect transistors and photodetectors). On the other hand, due to the 2D properties, the MoS_2–WSe_2 heterostructures' particular optical and electrical properties have broad prospects in the fields of small-scale, high-performance optoelectronic and nano devices. In addition, the direct band gap also makes MoS_2–WSe_2 heterostructures suitable for optical applications.

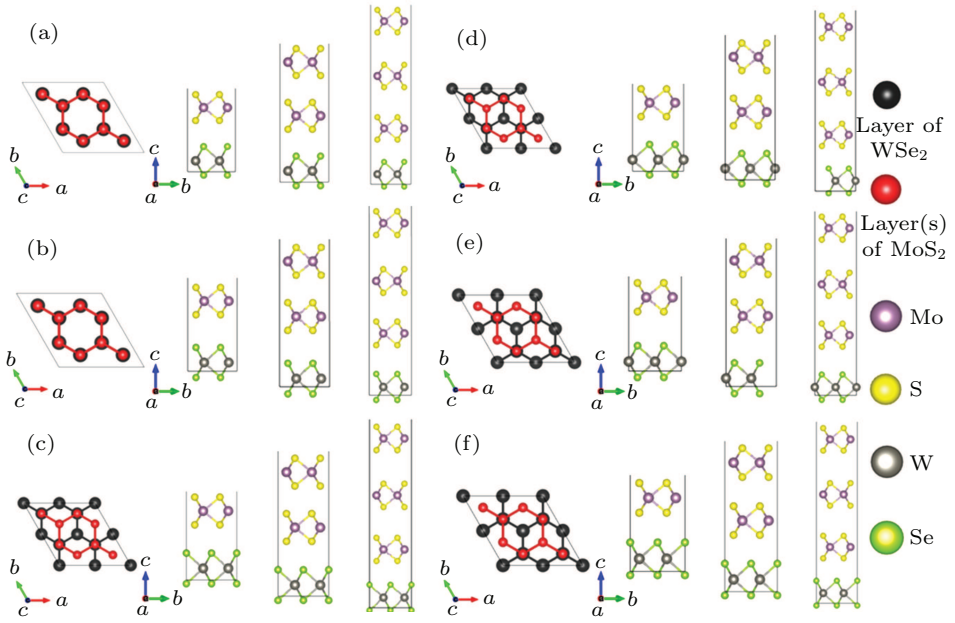


Fig. 2. Top and side views of WSe_2–MoS_2 heterostructures atomic model with six different stacking forms: (a)–(f) I–VI form stacking.

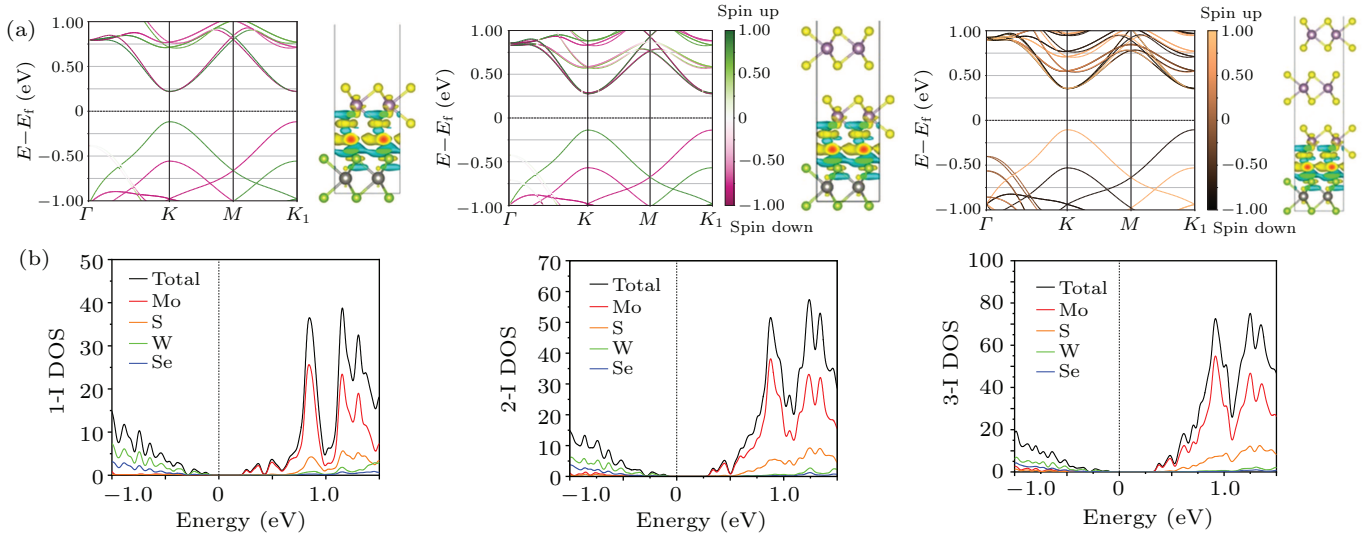


Fig. 3. (a) Computed charge density difference and band structure (with SOC) of type I stacking form WSe_2–MoS_2 heterobilayer, ML WSe_2–BL MoS_2 and ML WSe_2–TL MoS_2 heterostructures. (b) Density of states (DOS) of type I stacking form WSe_2–MoS_2 heterobilayer, ML WSe_2–BL MoS_2 and ML WSe_2–TL MoS_2 heterostructures from left to right.

Table 1. Calculated bandgaps (eV) of heterostructures composed of monolayer $MoSe_2$ and different thickness of 2H-MoS_2 in six stacking forms.

	I	II	III	IV	V	VI
ML WSe_2			1.185			
ML MoS_2			1.563			
ML WSe_2–ML MoS_2	0.338	0.255	0.313	0.257	0.259	0.378
ML WSe_2–BL MoS_2	0.410	0.337	0.393	0.345	0.337	0.466
ML WSe_2–TL MoS_2	0.447	0.368	0.440	0.388	0.373	0.495

3.2. Band engineering via magnetic moment

To investigate the effect of the z-axis magnetic moment at K/K_1 points, the $k \cdot p$ method and DFT are both adopted. At K/K_1 points, the Hamiltonian of all WSe_2–MoS_2 heterobilayers described by the $k \cdot p$ method can be written as[14]

$$\hat{H}_0 = at(\tau k_x \hat{\sigma}_x + k_y \hat{\sigma}_y) + \frac{\Delta}{2}\hat{\sigma}_z + \tau \begin{pmatrix} A & 0 \\ 0 & B \end{pmatrix} \hat{s}_z, \qquad (1)$$

in which $\tau = \pm 1$ is the valley index, a the lattice constant, t the effective hopping integral, Δ the band gap, $\hat{\sigma}$ the Pauli matrices for two basis functions, $\hat{s}$ the Pauli matrices for spin. The last term of Eq. (1) describes the SOC, where $|2A|$ and $|2B|$ deal with the spin split at conduction-band-edge and valence-band-edge (for monolayer MoS_2 and MoS_2–WSe_2 heterobilayers, $A = 0$). When considering an added z-axis magnetic field, the Hamiltonian reads

$$\hat{H}_1 = \hat{H}_0 + M_z \hat{s}_z. \tag{2}$$

Here, it should be noticed that the magnetic term is small and has not coupled with other terms. From which we can get the band edges at K/K_1 points: $\frac{\Delta}{2} + \tau A + M_z$, $-\frac{\Delta}{2} + \tau B + M_z$, $\frac{\Delta}{2} - \tau A - M_z$, $-\frac{\Delta}{2} - \tau B - M_z$. The first and third eigenvalues stand for the spin split in the conduction band edges while the second and fourth eigenvalues illustrate the spin split in the valence band edges. As mentioned above, the induced magnetic moment makes different band edges at K/K_1 points. In the situations of $A = 0$, CBMs have no difference at K/K_1 points with the rise of the magnetic moment, which still gives a direct bandgap. Generally speaking, the rising of magnetized term decreases the band gap.

Now, we have computed the WSe_2–MoS_2 heterobilayers with magnetic moment (z-axis) in the range of 0–0.15 μ_B (interval 0.03 μ_B). We list the bandgaps of all situations in Table 2 and show the computed band structures of 0.03 μ_B, 0.06 μ_B, 0.09 μ_B, 0.12 μ_B and 0.15 μ_B in Figs. 4 and S3.

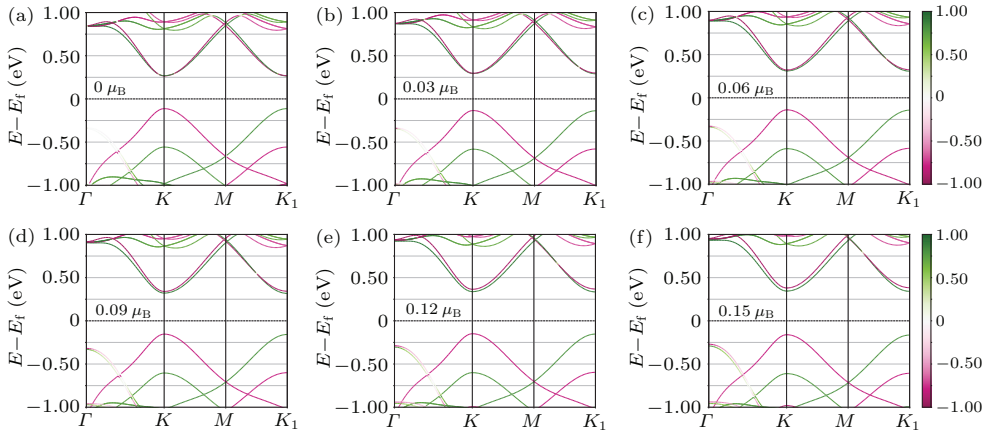


Fig. 4. Calculated band structures of magnetized VI form stacked WSe_2–MoS_2 heterobilayers with magnetic moment of (a) 0.00 μ_B, (b) 0.03 μ_B, (c) 0.06 μ_B, (d) 0.09 μ_B, (e) 0.12 μ_B, (f) 0.15 μ_B. Green and red colors indicate the spin-up and spin-down polarization.

Table 2. Calculated bandgap (in eV) of I–VI stacking WSe_2–MoS_2 heterobilayers with magnetic moments (ranging from 0 to 0.15 μ_B).

	I	II	III	IV	V	VI
0 μ_B	0.338	0.255	0.313	0.257	0.259	0.378
0.03 μ_B	0.390	0.345	0.366	0.315	0.348	0.421
0.06 μ_B	0.435	0.443	0.426	0.371	0.434	0.454
0.09 μ_B	0.454	0.538	0.446	0.408	0.529	0.470
0.12 μ_B	0.484	0.630	0.470	0.432	0.621	0.492
0.15 μ_B	0.497	0.670	0.485	0.452	0.652	0.501

As the difference of band edges between K and K_1 points is small, we use the difference between CBM and VBM as the band gap. As listed in Table 2, in all kinds of stacking types, the bandgap increases with the enhancement of the magnetic moment. Moreover, the tuning effect of magnetic moment depends on the stacking type. With a magnetic moment of 0.15 μ_B, more than 0.4 eV bandgap tuning appears in II-group stacking while I-group stacking only has a 0.159 eV bandgap regulation. For all six heterobilayers, the total free energies (without SOC) of I–VI type stackings are −181.189 eV, −180.845 eV, −181.110 eV, −181.166 eV, −180.859 eV, and −181.194 eV, respectively, in which types II and V have more advantages in the magnetized situations, they have similar total free energies ($\sim$ −180.8 eV). The total free energies of another group containing types I, III, IV and VI are all close to −181.2 eV, and the tuning effects on the bandgap of these stacking types are relatively close. Furthermore, the increase of magnetic moment raises a difference in band edges at K and K_1 points, which is similar to the results of the $k \cdot p$ method.

Compared with MX_2 (M = Mo/W, X = S/Se) monolayers, the multilayer situations are more complex due to the interlayer coupling. In the typical $k \cdot p$ method, the given systems are assumed to be fixed. In other words, the magnetic moments in this model should be very small to keep the system parameters (such as lattice constants and atom positions) unchanged which has negligible influence on the lattice. On the other hand, DFT calculations can consider larger magnetic moments due to full geometry optimization (coupling of the magnetic moment and the structure parameters). As a result, for a specific system, the $k \cdot p$ method is only applicable in a small range of magnetic moments, while the DFT calculation is suitable for a larger range of magnetic moment.

4. Conclusion and perspectives

In summary, we have performed a study of spin-valley polarization in six stackings of WSe_2–MoS_2 heterostructures

and magnetized bilayer systems by DFT. Calculations show that MX_2 monolayers and all six different stackings of WSe_2–MoS_2 heterostructures have direct-bandgap and valleytronics properties. Compared with MX_2 monolayers, the construction of WSe_2–MoS_2 heterobilayers achieves significant bandgap reduction (maximum 1.308 eV). On this basis, the rising thickness of 2H-MoS_2 can further regulate the band gap which depends on the stacking form. Furthermore, we have investigated the z-axis magnetized WSe_2–MoS_2 heterobilayers, both $k \cdot p$ method and DFT demonstrate that the z-axis magnetic moment introduces different band edges at K/K_1 points. For relatively larger magnetic moment, the band gap changes significantly. Similar to the thickness of 2H-MoS_2, the effect of the magnetic moment in band gap tuning also depends on the stacking type. As a result, the magnetic moment and thickness can be used as the further regulation means of stacking form to band engineering. Compared with previous studies, our methods are more effective and easier experimentally achieved. Our results suggest that WSe_2–MoS_2 heterostructures are suitable platforms for spin-valley applications due to their tunable direct bandgaps and valleytronics properties. In addition, thickness, stacking form and induced magnetic moment give controllable methods in the optical absorption of 2D multilayers, we believe our calculations are suitable for applications in 2D spin-valley nanostructures.

Acknowledgements

Project supported by the National Natural Science Foundation of China (Grant Nos. 61975224 and 12104004), the University Synergy Innovation Program of Anhui Province (Grant No. GXXT-2020-050), the Fund of Anhui Provincial Natural Science Foundation (Grant No. 2008085MF206), New magnetoelectric materials and devices, the Recruitment Program for Leading Talent Team of Anhui Province 2020, State Key Laboratory of Luminescence and Applications (Grant No. SKLA-2021-03), and the Open Fund of Infrared and Low-Temperature Plasma Key Laboratory of Anhui Province (Grant No. IRKL2022KF03).

References

[1] Gong C, Li L, Li Z L, Ji H W, Stern A, Xia Y, Cao T, Bao W, Wang C Z, Wang Y, Qiu Z Q, Cave R J, Louie S G, Xia J and Zhang X 2017 *Nature* **546** 265
[2] Huang B, Clark G, Navarro-Moratalla E, Klein D R, Cheng R, Seyler K L, Zhong D, Schmidgall E, McGuire M A, Cobden D H, Yao W, Xiao D, Jarillo-Herrero P and Xu X D 2017 *Nature* **546** 270
[3] Lee C H, Lee G H, Zande A M, Chen W C, Li Y L, Han M Y, Cui X, Arefe G, Nuckolls C, Heinz T F, Gou J, Hone J and Kim P 2014 *Nat. Nanotechnol.* **9** 676
[4] Pospischil A, Furchi A and Mueller T 2014 *Nat. Nanotechnol.* **9** 247
[5] Britnell L, Ribeiro R M, Eckmann A, Jalil R, Belle B D, Mishchenko A, Kim Y J, Gorbachev R V, Georgiou T, Morozov S V, Grigorenko A N, Geim A K, Casiraghi C, Neto A H C and Novoselov K S 2013 *Science* **340** 1311
[6] Jo S H, Ubrig N, Berger H, Kuzmenko A B and Morpurgo A F 2014 *Nano Lett.* **14** 2019
[7] Baugher B W H, Churchill H O H, Yang Y F and Jarillo-Herrero P 2014 *Nat. Nanotechnol.* **9** 262
[8] Mak K F, Lee C G, Hone J, Shan J and Heinz T F 2010 *Phys. Rev. Lett.* **105** 136805
[9] Splendiani A, Sun L, Zhang Y B, Li T S, Kim J, Chim C Y, Galli G and Wang F 2010 *Nano Lett.* **10** 1271
[10] Yao W, Xiao D and Niu Q 2008 *Phys. Rev. B* **77** 235406
[11] Mak K F, He K L, Shan J and Heinz T F 2012 *Nat. Nanotechnol.* **7** 494
[12] Zeng H, Dai J, Yao W, Xiao D and Cui X 2012 *Nat. Nanotechnol.* **7** 490
[13] Cao T, Wang G, Han W P, Ye H Q, Zhu C R, Shi J R, Niu Q, Tan P H, Wang E, Liu B L and Feng J 2012 *Nat. Commun.* **3** 887
[14] Xiao D, Liu G B, Feng W X, Xu X D and Yao W 2012 *Phys. Rev. Lett.* **108** 196802
[15] Shkolnikov Y P, Poortere E P D, Tutuc E and Shayegan M 2020 *Phys. Rev. Lett.* **89** 226805
[16] Zhu Z W, Collaudin A, Fauqué B, Kang W and Behnia K 2012 *Nat. Phys.* **8** 89
[17] Gunawan O, Shkolnikov Y P, Vakili K, Gokmen T, Poortere E P D and Shayegan M 2006 *Phys. Rev. Lett.* **97** 186404
[18] Sanchez O L, Ovchinnikov D, Misra S, Allain A and Kis A 2016 *Nano Lett.* **16** 5792
[19] Scharf B, Xu G F, Matos-Abiague and Žutić I 2017 *Phys. Rev. Lett.* **119** 127403
[20] Seyler K, Zhong D, Huang B, X L P, Wilson N, Taniguchi T, Watanabe K, Yao W, Xiao D, Mcguire M, Fu K and Xu X D 2018 *Nano Lett.* **18** 3823
[21] Zhao C, Norden T, Zhang P Y, *et al.* 2017 *Nat. Nanotechnol.* **12** 757
[22] Dong J and Ouyang G 2020 *Chin. Phys. B* **29** 086403
[23] Xu L, Lu W, Hu C, *et al.* 2020 *Chin. Phys. B* **29** 077304
[24] Yang H P, Yuan W J, Luo J, *et al.* 2019 *Chin. Phys. B* **28** 078106
[25] Hong X P, Kim J, Shi S F, Zhang Y, Jin C H, Sun Y H, Tongay S, Wu J Q, Zhang Y F and Wang F 2014 *Nat. Nanotechnol.* **9** 682
[26] Peng B, Yu G N, Liu X F, Liu B, Liang X, Bi L, Deng L J, Sum T C and Loh K P 2016 *2D Materials* **3** 025020
[27] Ceballos F, Bellus M Z, Chiu H Y and Zhao H 2014 *Acs Nano.* **8** 12717
[28] Ceballos F, Ju M G, Lane S D, Zeng X C and Zhao H 2017 *Nano Lett.* **17** 1623
[29] He J Q, Kumar N, Bellus M Z, Chiu H Y, He D W, Wang Y S and Zhao H 2014 *Nat. Commun.* **5** 5622
[30] Mishra r, Zhou W, Pennycook S J, Pantelides S T and Idrobo J C 2013 *Phys. Rev. B* **88** 144409
[31] Ramasubramaniam A and Naveh D 2013 *Phys. Rev. B* **87** 195201
[32] Cheng Y C, Zhu Z Y, Mi W B, Guo Z B and Schwingenschlögl U 2013 *Phys. Rev. B* **87** 100401
[33] Cheng Y C, Zhang Q Y and Schwingenschlögl U 2014 *Phys. Rev. B* **89** 155429
[34] Lu N, Guo H Y, Li L, Dai J, Wang L, Mei W N, Wu X J and Zeng X C 2014 *Nanoscale* **6** 2879
[35] Cheng C and Yan H Z 2009 *Physica E* **41** 828
[36] Li Y, Zhu H B, Wang G Q, Peng Y Z, Xu J R, Qian Z H, Bai R, Zhou G H, Yesilyurt C, Siu Z B and Jalil M B A 2018 *Phys. Rev. B* **97** 085427
[37] Li Y, Jiang W Q, Ding G Y, Peng Y Z, Wen Z C, Wang G Q, Bai R, Qian Z H, Xiao X B and Zhou G H 2019 *J. Appl. Phys.* **125** 244304
[38] MacNeill D, Heikes C, Mak K F, *et al.* 2015 *Phys. Rev. Lett.* **114** 037401
[39] Kresse G and Joubert D 1999 *Phys. Rev. B* **59** 1758
[40] Blochl P E 1994 *Phys. Rev. B* **50** 17953
[41] Kresse G and Furthmüller J 1996 *Phys. Rev. B* **54** 11169
[42] Perdew J P, Burke K and Ernzerhof M 1998 *Phys. Rev. Lett.* **77** 3865
[43] Grimme S 2006 *J. Comput. Chem.* **27** 1787
[44] Chang C H, Fan X F, Lin S H and Kuo J L 2013 *Phys. Rev. B* **88** 195420
[45] Ramasubramaniam A 2012 *Phys. Rev. B* **86** 115409